View metadata, citation and similar papers at core.ac.uk

brought to you by CORE

provided by NASA Technical Reports Server

COMPARISON OF MEASURED AND CALCULATED DYNAMIC LOADS FOR THE MOD-2 2.5 MW WIND TURBINE SYSTEM

N95-27983

D. K. Zimmerman, S. A. Shipley and R. D. Miller

Boeing Aerospace Company
Seattle, WA 98124

ABSTRACT

The Boeing Company, under contract to the Electric Power Research Institute (EPRI), has completed a test program on the Mod-2 wind turbines at Goodnoe Hills, Washington. The objectives were to update fatigue load spectra, discern site and machine differences, measure vortex generator effects and to evaluate rotational sampling techniques. This paper shows the test setup and loads instrumentation, loads data comparisons and test/analysis correlations. Test data is correlated with DYLOSAT predictions using both the NASA interim turbulence model and rotationally sampled winds as inputs. The latter is demonstrated to have the potential to improve the test/analysis correlations. The paper concludes with an assessment of the importance of vortex generators, site dependence, and machine differences on fatigue loads. The adequacy of prediction techniques used are evaluated and recommendations are made for improvements to the methodology.

BACKGROUND

The Boeing Company, under contract to the Electric Power Research Institute (EPRI), conducted a loads development and rotational sampling test program on the Mod-2 wind turbines located at Goodnoe Hills, Washington. The test period was from June through August, 1983. These 300-foot diameter, 2500 kW, horizontal-axis wind turbines were developed for DOE/NASA, began operation in January, 1981 and were integrated into the Bonneville Power Administration (BPA) utility grid in June, 1982. Identical units are owned and operated by the Bureau of Reclamation (BuRec) in Medicine Bow, Wyoming and Pacific Gas and Electric Company (PGandE) in Solano County, California.

Since the completion of Mod-2 acceptance tests in June, 1982, wind turbine stability and performance had been improved with a new control algorithm and addition of vortex generators (VG) on the rotor blades. Little data on the effect of these changes on fatigue loads were available. Requirements for additional loads instrumentation were also recognized. The objectives of the loads development test were to collect loads data on the major structural subsystems in order to update the Mod-2 loads data base, to refine the fatigue load spectra and to update fatigue life projections. Site dependency was also investigated by comparing test data from the Goodnoe Hills and Solano units. The adequacy of loads and fatigue life methodology was evaluated, addressing such issues as fatigue cycle counting methods and load phasing.

Previous tests also revealed that some of the analytic fatigue load prediction techniques used during the Mod-2 design needed improvement. The cyclic loads due to deterministic sources such as wind shear, upwind tower shadow, yaw error and gravity loading were reasonably well understood and predicted adequately. The most notable shortcoming was the inability to predict accurately the dynamic response to turbulence and its variations across the rotor disk. In conjunction with Pacific Northwest Laboratories (PNL), Boeing also completed a rotational sampling test program funded by EPRI aimed at improving test/analysis correlations. Unit #2 at Goodnoe Hills was used to measure wind velocities at several locations on the rotating rotor. These were used as input to a computer simulation of the wind turbine (DYLOSAT) to predict structural loads. A comparative analysis of the predicted loads with actual test data was made, to develop a better understanding of wind turbulence and to assess the ability of DYLOSAT to predict cyclic loads.

TEST DESCRIPTION

System Description

A photo of the Goodnoe Hills site is shown in Figure 1. Looking west, the Mod-2 wind turbines are designated (left to right), Unit #1, Unit #3 and Unit #2. The general arrangement and characteristics of the Mod-2 configuration are shown in Figure 2. It is designed for operation at sites where the annual average wind speed is 14 mph measured at 30 feet (20 mph @ hub height). The wind turbine generates electricity when the wind speed at hub height (200 feet) exceeds 14 mph. For winds exceeding 27.5 mph, the system produces rated power of 2500 kW.

Test Configuration

The loads development tests were performed on Units #2 and #3. Vortex generators were installed to improve aerodynamic stability and increase performance. Unit #2 had vortex generators installed on the blade midsections (70% VG) throughout the entire test program. Unit #3 started the test with no VG and subsequently had VG installed on the midsection (70% VG) and tip (100% VG). The vortex generators on the midsection and tip are illustrated in Figure 3.

The control system had been improved considerably since acceptance testing, during which the system occasionally exhibited dynamic instability due to aerodynamic nonlinearities at the peak of the power-blade angle curve. Control system improvements were incorporated into Units #2 and #3 before the start of loads development testing.

Test results from Units #2 and #3 were compared with data from a previous test on the PGandE machine (Unit #5) at Solano, California. This wind turbine had 70% VG and was identical to the Goodnoe Hills units except for a slight difference in nominal pitch schedule in below rated wind speed.

The rotational sampling tests were performed on Unit #2 concurrent with the loads development test.

Test Instrumentation

To meet the objectives of the loads test program, approximately 53 new loads and strain channels were added. The primary new instrumentation included additional flapwise bending loads in the rotor, pitch actuator force, nacelle pitch and yaw bending, upper tower bending and yaw drive torque. Figure 4 shows the location of the critical load measurements monitored in this test program.

Instrumentation for the rotational sampling test included the existing engineering instrumentation and special instrumentation (16 channels) installed on the rotor. The special rotor instrumentation included wind flow probes mounted at the leading edge of the blades at Stations 360 and 1205, and a differential pressure probe mounted on the trailing edge of one blade at Station 1120. In addition, accelerometers were located at Stations 360 and 1209 on one blade and a temperature transducer at Station 1205 on Blade 2.

Real time evaluation of the wind stability conditions was made by PNL, derived from an acoustic sounder located 3 diameters upwind of Unit #2. The acoustic sounder provided measurement of wind velocity over the elevation from 30m to 220m above the ground at 10m intervals.

A layout of the test data center is shown in Figure 5. Data from the wind turbines under test and meteorological data from the BPA and PNL towers were transmitted via the existing intra-site system to the data center adjacent to Unit #2. The data center recorded the data on analog tape and also transmitted the data to the NASA mobile data system (MDS). A digital data system (DDAS) supplied by Boeing provided on-site data processing capability for the calibrations and the loads development tests. Data was also digitized at the PNL trailer for the rotational sampling tests.

Wind Observations

Earlier wind turbine testing identified the need to develop a systematic scheme to sort loads data, accounting for the changing wind turbulence and gradient conditions observed during a test. A wind code defining the turbulence and wind gradient, similar to that employed by PGandE for performance evaluation, was used to sort cyclic loads data at both the Goodnoe Hills and Solano sites (Figure 6). Although this effort was not completely successful because of the distance of the met towers from the wind turbines, it was demonstrated that the Solano site experienced high shear/low turbulence and the Goodnoe Hills site high shear/high turbulence during their test periods. The higher turbulence levels appeared to be associated with higher cyclic loads observed at the Goodnoe Hills site. It was also demonstrated that the wind conditions observed at Goodnoe Hills were characteristic of both seasonal (summer) and annual conditions. The loads development tests and rotational sampling tests were run in parallel in winds of opportunity, ranging up to 38 mph at hub height.

LOADS DATA EVALUATION

Loads data recorded on magnetic tape at the data center were digitized and processed in real time at the DDAS. Raw data were monitored in real time on brush records. Data for each load channel was collected over 5-minute intervals and digitized at 10 samples per second. This sample rate was sufficient to cover responses through 4 per rev, which included the fundamental frequencies of the tower (1.26 per rev), drive train (0.45 per rev) and rotor flapwise mode (3.72 per rev). Typical digitized data traces are shown in Figure 7.

Data were reduced to the form of summary wind bins plots and tabular output. A total of 724 8-inch floppy discs (5 minutes, 9 channels each) were obtained. Each disc contained the digitized data for the run, atmospheric temperature and pressure, wind code and processed fatigue loads corrected to standard sea level conditions.

Although summary loads data in raw form were available as an output of the test phase, further data manipulation was required to differentiate site and machine differences, determine the effect of vortex generators and to assess the usefulness of sorting by the wind code. These tasks involved curve fitting scattered data, extrapolating to higher winds, cross plotting and sorting.

Site and Unit Differences

Pretest predictions of mean loads with the current control laws were updated using the DYLOSAT computer program. Both DYLOSAT predictions and test data confirmed that loads for Unit #5 tended to be lower than Units #2 and #3 due to small pitch schedule differences. Pretest predictions of cyclic loads using DYLOSAT were not made because of inability to prescribe proper turbulence inputs to the model.

DYLOSAT predictions generally correlated well with mean flapwise loads data, as shown in Figures 8 through 17. Both predictions and test data show the effects of pitch scheduling: slightly decreasing pitch angle up to 20 mph, constant pitch from 20 to about 27 mph (rated wind speed), and rapidly increasing pitch angle to hold rated power above 27 mph. The data scatter is typical of that observed in previous tests and at least partially due to plotting loads versus met tower wind speed, which is known to differ from that at the wind turbine by approximately $\pm$ 2 mph. Flapwise load data measured at the same station but on opposite blades were very consistent for Units #2 and #3. Data from Units #2 and #3 were in good agreement in below-rated winds, although small variations were noted in above-rated winds, probably due to small aerodynamic differences between the rotors. Mean flapwise loads for Unit #5, shown in Figure 10, tended to be lower than Units #2 and #3 because of the difference in pitch schedule.

The pitch control actuator force was measured on Units #2 and #3 but not on Unit #5. On both Units #2 and #3 actuator force was deduced by using the pressure differential from the rod to the head end, a technique employed during Mod-2 acceptance testing. In addition, on Unit #3 the actuator rod eye was instrumented and calibrated to read rod force directly (01L301)to verify the previous measurement technique.

The mean actuator rod force for Unit #3 is shown in Figure 13. The pretest predictions shown were based on very limited test data obtained during Mod-2 acceptance testing. Very good correlation was obtained by the two measurement techniques on Unit #3, validating the previous method.

A comparison of test data and DYLOSAT predictions for mean quill shaft torque are shown in Figures 14 and 15. These plots are equivalent to performance plots (power versus wind speed). The latter are usually developed from smooth wind data, however, to minimize data scatter. Neverthless, the quill shaft data is in fair agreement with DYLOSAT predictions. The data suggest that Unit #2 performance is slightly better than Unit #3. Unit #2 appears to reach rated torque at 27 mph and Unit #3 at 28 mph.

The mean tower bending moment data is compared to DYLOSAT predictions in Figures 16 and 17. The data are the vector sum of bending about two horizontal axes at Sta. 600. DYLOSAT predictions appear to be somewhat higher than data, particularly at near-rated wind speed. Unit #2 data also is slightly higher than Unit #3, indicating that the mean thrust and performance of Unit #2 should be higher.

Cyclic flapwise load data for Unit #2 and #3 with 70% VG were very similar. Curve fits to the cyclic loads data at Sta. 370 on Unit #2 are shown in Figure 18. The curve fits are based on trends predicted by the DYLOSAT program, using the NASA interim turbulence model as input, amplitude adjusted to fit the measured data.

Cyclic load data for Unit #5 was curve fitted in a similar manner. The mean cyclic flapwise load data for Units #2, #3 and #5 are compared in Figures 19. There is good agreement between the recent data for Units #2 and #3 and acceptance test data. The differences are mainly due to the type of curve fit employed. During acceptance testing a power law fit with wind speed was assumed; for the loads development test the curve fits were based on DYLOSAT trends. There is a clear difference in cyclic loads between Goodnoe Hills and Solano. Solano cyclic loads were approximately 20 percent lower at all wind speeds.

Tower cyclic loads at Sta. 600 are compared in Figure 20. The recently measured tower cyclic loads on Units #2 and #3 are higher than acceptance test. Recent control system changes may have resulted in control system response more closely coupled to the tower mode, which would increase the tower response. Unit #5 cyclic tower loads are approximately 20 percent lower than Units #2 and #3, most likely due to the lower turbulence at the Solano site.

The cyclic teeter angles during operation for all units are compared in Figure 21. The teeter data was similar to acceptance test data indicating 70 percent VG have not adversely affected teeter response. The expected high teeter response for Unit #5 due to severe wind gradient characteristic of the Solano site did not materialize. Severe gradients occasionally did occur during the test period at Solano, but did not affect the teeter response statistics.

Vortex Generator Effects

The effect of VG was evaluated by comparing mean and cyclic load data on Unit #3 for three VG configurations. Data analysis concentrated on determining variations in rotor flapwise loads and drive train loads. Statistical analysis of the mean and cyclic data for 5-minute intervals was performed on site at the DDAS. To determine the effect of VG on performance more accurately, 10 minute averages in smooth wind conditions were later processed in Seattle.

Curve fits to the mean flapwise loads data at Sta. 370 are compared in Figure 22. Unit #3 with 0% VG was unable to achieve rated power below 34 mph. This resulted in a continued increase of flapwise moment with wind speed because the blade could not unload to spill power. With the addition of 70 percent VG, however, Unit #3 reached rated power at a lower wind speed. In above-rated winds, the mean flapwise loads decreased as the collective pitch increased significantly to spill power. For below-rated wind, a slight increase in mean flapwise loads was noted for 70% VG compared to 0% VG. A small increase was also noted in mean load between 70% and 100% VG.

Unlike the mean loads, the cyclic loads data for both 5 and 10 minute data samples failed to reveal any statistically significant difference in cyclic loads for different VG configurations.

Improved performance with vortex generators is discussed in Reference 1. A typical performance plot is illustrated in Figure 23.

Comparison of Fatigue Counting Methods

Existing fatigue cycle counting procedures include the method used on Mod-2, NASA wind bins based on 1P sampling, rainflow, and others. The Mod-2 method was selected for compatibility with the fatigue life methodology being followed. As part of loads methodology assessment, the Mod-2 fatigue counting method using the DDAS was compared with a rainflow procedure using the Datamyte 400. This device is a solid state, software controlled histogram processor/recorder used for field recording of analog data (one channel at a time). A major advantage of the Datamyte 400 is its ability to process and store large quantities of data spanning months of testing.

The Mod-2 fatigue cycle counting method determines the major cyclic load excursions about a mean load, ignoring minor reversals and a prescribed dead band (Figure 24). It is believed that addition of these loads to long period load cycles due to a varying mean wind and startup/shutdown load cycles fairly represents the fatigue load damage potential.

The Datamyte rainflow algorithm has the potential to produce superior fatigue life estimates and still is compatible with current fatigue life methodology. The rainflow algorithm is a range-pair method but counts only those cycles which complete a hyteresis loop, as shown in Figure 25. It produces a histogram format of cyclic data which can be correlated with cumulative probability and exceedance distributions produced by current methods.

The cumulative distribution of the flapwise cyclic load at Sta. 370 over a 5 minute interval is shown in Figure 26. The 50 percentile level by the Mod-2 method is consistent with the Datamyte rainflow algorithm, but the 0.999 percentile level is lower. The most notable difference in the two methods is the shape of the cumulative distributions. The Datamyte 400 results are clearly non-Gaussian. This trend persists for 20 minute data samples as well.

The comparison of the two methods of counting load cycles is presented in a form more useful for fatigue life analysis in Figure 27. This plot shows the number of exceedances of a certain load level and reflects not only the difference in the distribution but also the difference in the total number of fatigue cycles counted. Although there is generally good agreement, the tails of the distributions are different, suggesting the present method is somewhat unconservative for low probabilities of occurrence.

ROTATIONAL SAMPLING TEST/ANALYSIS CORRELATION

The rotational wind sampling test was conducted by Boeing and directed by PNL with the objective of developing an improved wind model. Following the test, PNL reduced and analyzed the wind data (Reference 2); PNL results were used in the Boeing analysis. The wind model is required as input into the improved theoretical aeroelastic computer program (DYLOSAT) that Boeing has developed for calculating dynamic loads on the wind turbine. This study assessed the suitability of the wind model and the DYLOSAT program to predict dynamic loads by comparing analysis with loads measured in the rotational wind sampling test.

Analytic Methods

The analytic model of the wind turbine system consists of a matrix of second order non-linear differential equations of the form

$$[M(t)]\ddot{q} + [c(t)]\dot{q} + [k]q = F(t) \qquad (1)$$

where the forcing function F(t) is derived from theoretical aerodynamics and a wind description. A computer code (DYLOSAT) was developed to calculate the aerodynamic forcing function from a description of the wind, to formulate load equations and to solve the equations of motion and load equations. A sketch of the DYLOSAT model is shown in Figure 28.

Equation (1) can be solved in either the time or the frequency domains. For both of these solutions, the aerodynamic model is based on a strip momentum rotor analysis developed on a finite number of spanwise segments. Finer segments are used near the tip to increase numerical accuracy because the aerodynamic forces (resulting in rotor loads and hub torque) are concentrated towards the tip.

Calculating the aerodynamic forces on each segment requires definition of the wind turbulence at each segment. Much of this study was devoted to assessing two wind turbulence models (the NASA interim turbulence model and the rotationally sampled wind turbulence model) and two solution methods (frequency response analysis and time history analysis).

a) The NASA Interim Turbulence Model

The NASA interim turbulence model is based on wind data collected by PNL at Clayton, New Mexico from a vertical plane array of anemometers on several meteorological towers. The NASA Lewis Research Center used the wind turbulence spectrum from this data to develop a non-dimensional curve as a function of rotor speed harmonics (Figure 29). Using this non-dimensional curve with the empirical equations shown below, the rms turbulence wind velocity amplitude can be calculated at specified steady state wind velocities and rotor speed harmonics.

$$V(.75r,\psi) = V_o + \delta V_s(V_o,\ .75r/h_o) \sum \frac{\cos(n\psi i)}{n + 0.75}$$

where

$V(.75r,\psi)$ = wind speed at 75% rotor radius r and rotor azimuth ψ
$V_o = V(o,\psi)$ = wind speed at hub height
$\psi_i = \psi$ for blade 1, $\psi + \pi$ for blade 2
$\delta V_s = V_o\,[1 + .75\ r/h_o)^{\alpha} - (1 - .75\ r/h_o)^{\alpha}]$
$\alpha = .35\,[1 - .55 \log (V_o)]/[1 - .19 \log (h_o/10)]$
h_o = hub elevation
n = harmonic number

The cyclic wind velocity is assumed to vary linearly with rotor radius from zero at the hub to a maximum at the tip. From a large amount of Mod-2 wind turbine test data, using $\alpha = .24$ for all wind speeds produced the best data fit. Consequently, this value of α was used for this study. Utilizing random harmonic analysis techniques, the wind is assumed to act sinusoidally on the blade at each harmonic frequency as shown conceptually in Figure 30. The sinusoidal wind turbulence is assumed to be completely in-phase over the total blade. For the two blades, the sinusoidal wind turbulence is assumed in-phase on each for the even harmonics and 180° out-of-phase for the odd harmonics. These rms turbulence wind velocity amplitudes were used in calculating the turbulence induced aerodynamics of the forcing function.

b) Rotationally Sampled Wind Turbulence Model

The wind velocity was measured dynamically at four blade locations, Stations 360 and 1206, on both blade 1 and 2 as shown conceptually in Figure 31. Wind spectra as a function of rotor speed harmonics were calculated by PNL from time segments of the wind data collected at each of the measurement stations. This yielded the rms wind turbulence velocity amplitude spectra at four stations on the rotor. In addition, cross spectra between measurement stations of the wind data were calculated to yield the phase relationship between the spectra as a function of rotor speed harmonics.

The rotationally sampled wind turbulence model has in concept refined the NASA interim turbulence model from one wind turbulence spectrum used on both blades to four wind turbulence spectra on the rotor and the phase angle relationship between each spectra. The velocity amplitude and phase relationship at any other station on the rotor is assumed from linear interpolation or extrapolation of the spectra data on each blade.

c) Frequency Response Analysis

Frequency domain analysis of the equations of motion is similar to the power spectral density technique that utilizes random harmonic analysis. The equations are solved for steady state solutions from a series of sinusoidal forcing functions of ω, $\omega + \Delta\omega$, $\omega + 2\Delta\omega$, etc., with magnitude equal to the square root of the forcing function spectrum at the respective frequencies. Because the equations are nonlinear, classical methods of solving for the particular solution of the second order differential equations could not be used. The method used was to solve the equations as a time history solution with a sinusoidal forcing function of the correct magnitude and frequency. From the time history solution, the steady state cyclic amplitude for the corresponding forcing function frequency is obtained and produces one solution point for that frequency. Solutions over the frequency range of interest for the wind turbine comprise the frequency domain analysis. In the case of the load equations, the load output spectrum is also obtained by this method and the rms loads are obtained by integrating the load output spectra. Because, the loads on a wind turbine are primarily caused at harmonics of the rotor speed, the equations of motion and load equations were only solved at the harmonics (1P → 5P).

d) Time History Analysis

The time history analysis involves numerical integration of Equation (1) with the actual wind wind turbulence time histories used as input for the forcing function. Loads and responses as a function of time are obtained as part of the solution. A spectral analysis of the resulting time histories was used for determining the frequency and amplitude content of the load. The response time histories were also compared to test data.

Results and Discussion

The data collection and data reduction of the rotationally sampled wind data was performed by PNL and reported in Reference 2. From the large quantity of test data recorded, PNL reduced four cases of data segments of approximately eight minutes each from which three cases were chosen for use in this analysis. The three cases analyzed are shown in Table 1.

a) Rotationally Sampled Wind

The rotationally sampled wind turbulence spectra for case 1 (a typical case), for the four blade test locations, are shown in Figure 32. The rotationally sampling wind instrumentation measured wind fluctuations from two sources, the turbulence in the wind (including variations due to the blade rotating through the turbulent eddies), and the variations due to the blade rotating through wind shear. This latter source shows up in spectral plots primarily at the 1P harmonic of the rotor rotational speed. Examining the spectrum in Figure 32 shows that the magnitude at 1P is significantly larger than the higher harmonics. Since the instruments at stations 1205 rotate through a larger range of wind shear than those at stations 360, it would be expected that the trend of the turbulence spectrum being highest at the first harmonic compared to the higher harmonics would be more pronounced for stations 1205 than 360, but this was not observed. The instruments on both blades follow the same track so there is good agreement between the two blades as shown in Figure 32.

The coherence of two signals is a good indication of the usefulness of the cross spectrum for use in a frequency domain analysis. A low coherence indicates that the two signals are uncorrelated and although a cross spectrum and a phase angle relationship can be calculated, the results have little significance. Figure 33 presents the coherence of the signals at the four test stations referenced to the signal from the instruments on blade 2 at station 1205. From Figure 33 it is apparent that the signals are uncorrelated for most harmonics. The coherence of the first harmonic is high probably because of the velocity fluctuations from rotating through the shear layers, which should produce highly correlated signals. If the velocity fluctuations from rotating through shear were removed from the signals, the coherence for just the turbulence signals would most likely be very low at all harmonics.

The low coherence indicates that the correlation between signals is poor and the calculated phase angles between stations and as a function of harmonics are not valid. Unfortunately, the phase angle relationship between wind spectra is important for frequency domain analyses and greatly affects the load calculations.

b) Frequency Domain Loads Analysis

Bending moment loads were calculated at rotor station 370 and 1164 by DYLOSAT with the NASA interim turbulence model and the rotationally sampled turbulence wind model; results were compared to experimentally measured loads for the three cases. Because the phase angles from the rotationally sampled wind were meaningless, only the wind spectra were used as input to DYLOSAT. The phase angle relationship of the wind on each blade and between blades was assumed to be the same as for the NASA interim turbulence wind. That is, the wind was in-phase at all points on a blade and was in-phase between blades for the even harmonics and 180° out-of-phase between blades for the odd harmonics. Figure 34 presents the bending moments for case 1.

The total bending moment is also shown in this figure. The total load is calculated as the root-sum-square of the first through fifth harmonics. It is apparent that the rotationally sampled wind model produces results considerably higher than the NASA interim turbulence model or test results. These loads can be attributed to the lack of a phase angle relationship between the wind measurement stations and that a worst case phase angle relationship was assumed for the even harmonics from which most of the load is associated.

The NASA interim turbulence model produces results that are closer to test in some cases and not as close in others, compared to the rotationally sampled wind. There appears to be no consistency in the results; using either wind turbulence model for calculating absolute loads for design purposes would be risky. The lack of phase angle relationships between the wind spectra precludes using these techniques for calculating absolute loads. Their use can only be justified when determining trends in the loads.

c) Time History Loads Analysis

The time history analysis of DYLOSAT to calculate structural loads is the most direct approach in the use of DYLOSAT. The rotationally sampled wind is directly input into the computer program to force the wind turbine model at the appropriate test locations on the rotor. The time history bending moment loads from DYLOSAT can be directly compared to the bending moment loads recorded during testing. Figures 35 through 37 shows a twenty second segment for Case 1 of the bending moment test results and the predictions for rotor stations 370 and 1164 and tower station 600. Comparing the test and analysis results shows a definite correlation between the time history signals. Although the signals do not match identically, the characteristics are similar.

Comparisons of the spectral content of the time history analyses and data are shown in Figures 38 and 39. From these figures, the frequency content of the analysis and test agrees very well for the rotor up to the first blade bending frequency of approximately 1.2 Hz. For frequencies above 1.2 Hz, the agreement deteriorates because the theoretical model of the rotor has only one asymmetric mode above 1.2 Hz. The amplitudes of the spectra from the analysis tend to be higher throughout the spectra. This can be attributed to the lack of sufficient rotationally sampled wind time series to define the wind turbulence adequately over the rotor. With only two test locations on each blade, the theoretical model required a linear interpolation and extrapolation of the wind time history signals to define the wind over the entire blade. This effectively defines the wind as being highly correlated between the test data and the interpolated data which would produce higher load predictions.

CONCLUSIONS AND RECOMMENDATIONS

The loads development test program was considered successful when measured against the primary program objective. A significant improvement in the Mod-2 fatigue loads data base was accomplished, providing more accurate Mod-2 fatigue life estimates than previously available. Although the full matrix of wind gust and gradient conditions could not be completed, the data obtained was shown to be typical of the Goodnoe Hills site. Data gathered during the test program was adequate for the purpose of evaluating site and machine differences and the effect of VG on loads and performance.

The most important output of the test program was refinement of the fatigue load spectra compared to acceptance test results. Mean loads data were shown to be in good agreement with predictions, validating use of the DYLOSAT computer program for this purpose. Cyclic load distributions were refined based on the additional load channels monitored in this program, improved calibration and data processing methods.

Test data provided insight into machine and site differences and the effect of VG on loads and performance. Little difference in loads was noted between similar machines at the same site. Variations in turbulence levels and wind gradient were found to be more relevant. Cyclic load levels between Solano and Goodnoe Hills were found to differ by approximately 20%, attributable to the difference in turbulence levels. The addition of VG was demonstrated to improve performance, increase mean loads for below-rated wind speeds, decrease mean loads for above-rated wind speeds, but have little effect on cyclic loads.

The analysis explored several loads methodology concerns including fatigue cycle counting methods, load/strain correlation and load phasing. The Datamyte 400 (rainflow) algorithm was shown to be more severe than present methods, which may affect fatigue life estimates. On the other hand, load/strain correlations indicate that loads/stress methodology was otherwise very conservative.

Although the loads development tests met many program objectives, the data review and methodology assessment revealed several deficiencies. Some of these deficiencies may be overcome simply by extension of the testing program to longer periods of time. Others were more fundamental in nature, suggesting a need to modify present methods or to adopt new approaches yet to be defined. In particular, sorting of cyclic loads data by a simplified wind gradient/turbulence code needs to be developed. To reduce data scatter, improved methods of averaging data such as disc averaging need to be developed. Various fatigue cycle counting methods should be evaluated over the short and long term.

The rotational sampling test results showed that much work remains to develop an acceptable wind turbulence model. Based on the cross spectral analyses and low coherence between the wind time series, there is much less correlation in the wind between spatial locations than that used in the NASA interim turbulence model and the similar approach taken when using the rotationally sampled wind data. The turbulence of interest appears smaller in length than the distance between measurements, giving very little spatial correlation. Utilizing rotationally sampled wind turbulence spectra is difficult because of this low coherence.

Using the time series of the rotationally sampled wind directly with DYLOSAT shows more promise. Correlation of the spectral analysis of the time series from test and DYLOSAT was fair and could be much improved with more closely spaced test stations or a better interpolation scheme. Only a better defined wind model is required until design cyclic loads can be predicted analytically with confidence. The wind model must be able to define turbulence on the rotor with the observed spectra characteristics and low coherence. If possible, this detailed definition should be derivable from meteorological tower data using only a few measurements locations.

REFERENCES

1. Miller, G. E.; "Comparative Performance Tests on the Mod-2, 2.5 MW Wind Turbine With and Without Vortex Generators," Horizontal-Axis Wind Turbine Technology Workshop sponsored by DOE/NASA, Cleveland, Ohio, May 8-10, 1984.

2. Connell, J. R; George, R. L.; Sandborn, V. A.: "Rotationally Sampled Wind and Wind Turbine Response at Goodnoe Hills Mod-2, Unit No. 2, Measured in July-August, 1983: A Preliminary Analysis", Research Project RP 1996-12, PNL, December 1983.

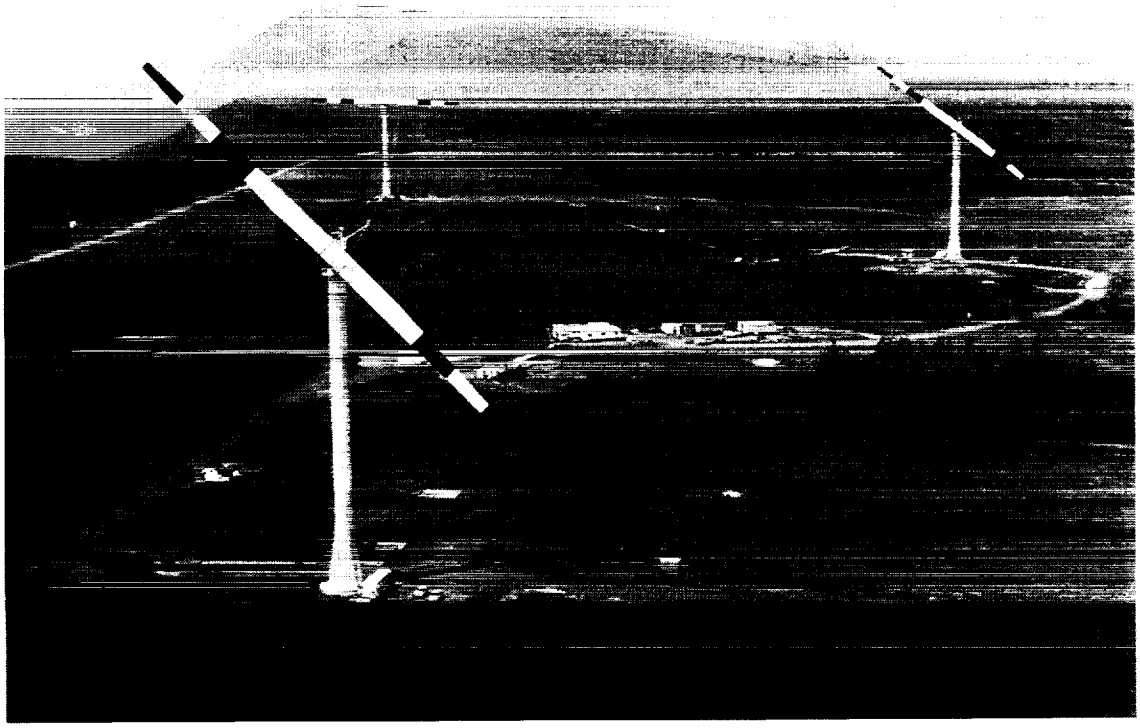

Figure 1. Mod-2 Wind Turbine Site at Goodnoe Hills, WA

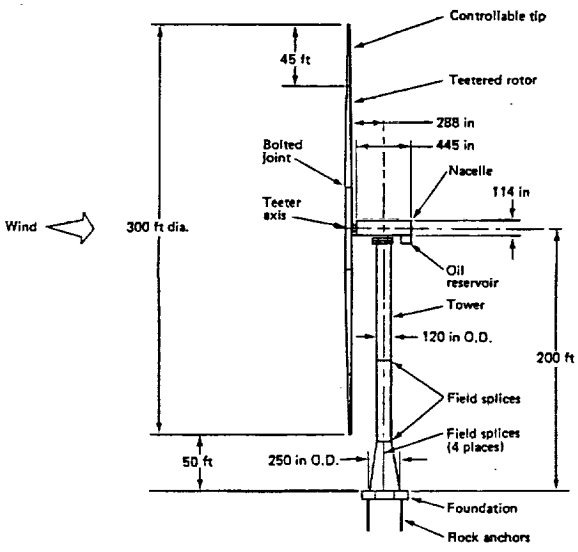

Rated power	2,500 KW
Rotor diameter	300 ft
Rotor type	Teetered - tip control
Rotor orientation	Upwind - 2.5° tilt
Rotor airfoil	NACA 230XX
Rated wind @ hub	27.5 mph
Cut-off wind speed @ hub	45 mph
Rotor tip speed	275 ft/sec
Rotor rpm	17.5
Generator rpm	1,800
Generator type	Synchronous
Gear box	Compact planetary gear
Hub height	200 ft
Tower	Soft-shell type
Pitch control	Hydraulic
Yaw control	Hydraulic
Electronic control	Microprocessor
System power coefficient (max)	0.382

Figure 2. Mod-2 Features and Characteristics

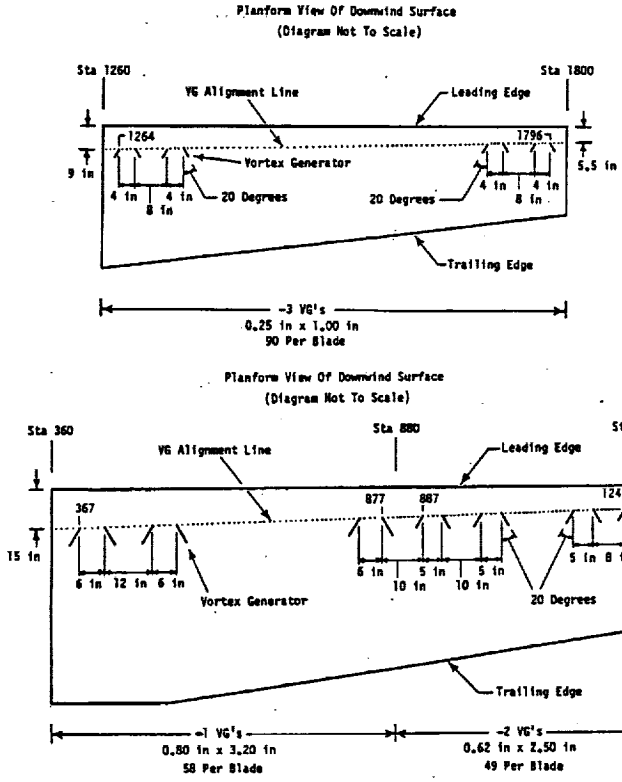

Figure 3. Vortex Generator Installation on Mod-2 Blade

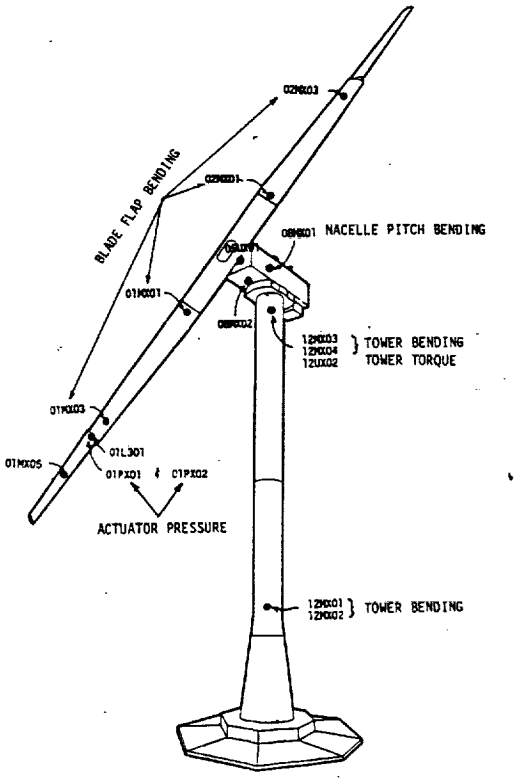

Figure 4. Critical Load Measurements

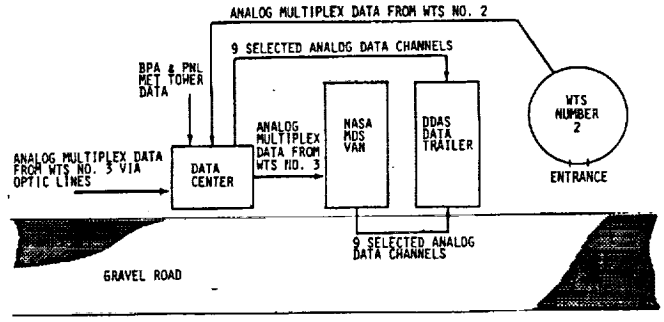

Figure 5. Layout of Test Data Center

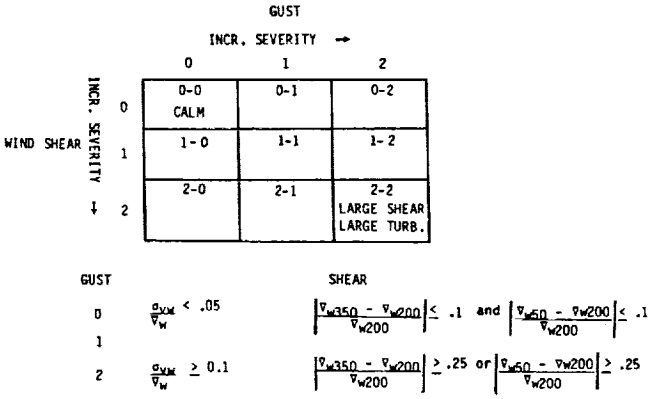

Figure 6. Wind Code

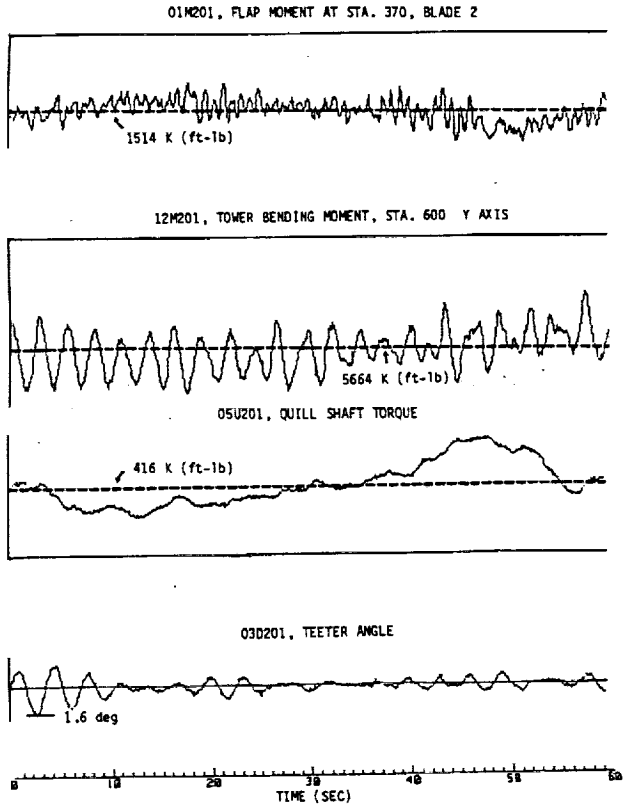

Figure 7. Typical Data Traces

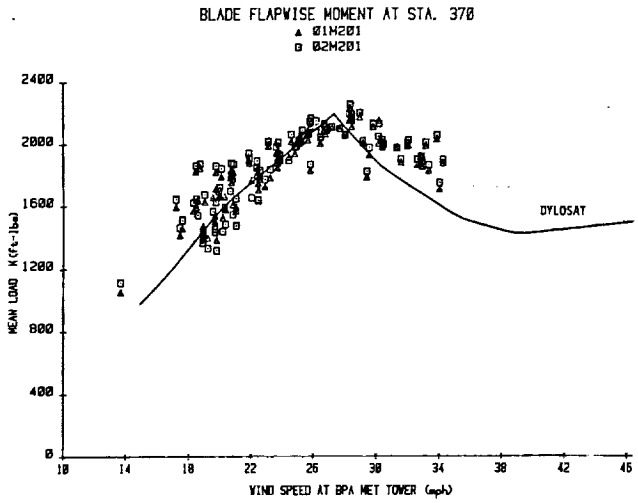

Figure 8. Mean Flapwise Moment at Sta. 370 (Unit #2, 70% VG)

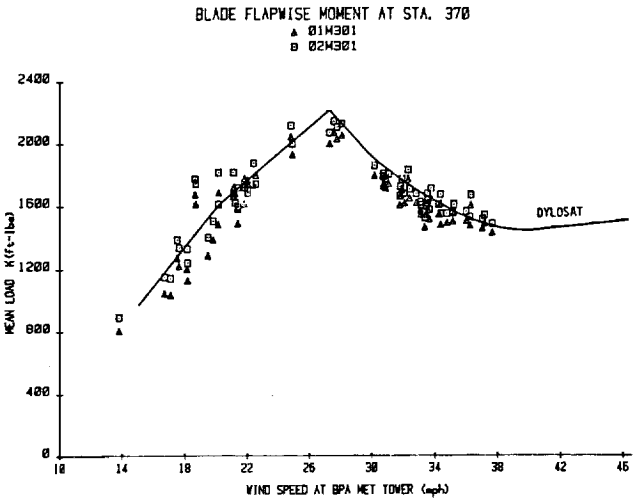

Figure 9. Mean Flapwise Moment at Sta. 370 (Unit #3, 70% VG)

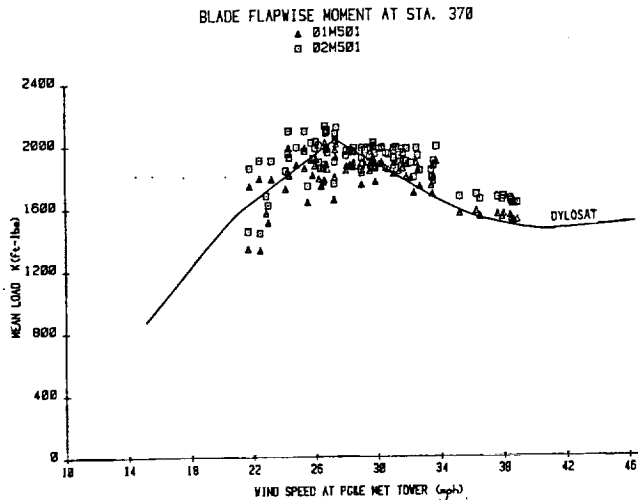

Figure 10. Mean Flapwise Moment at Sta. 370 (Unit #5, 70% VG)

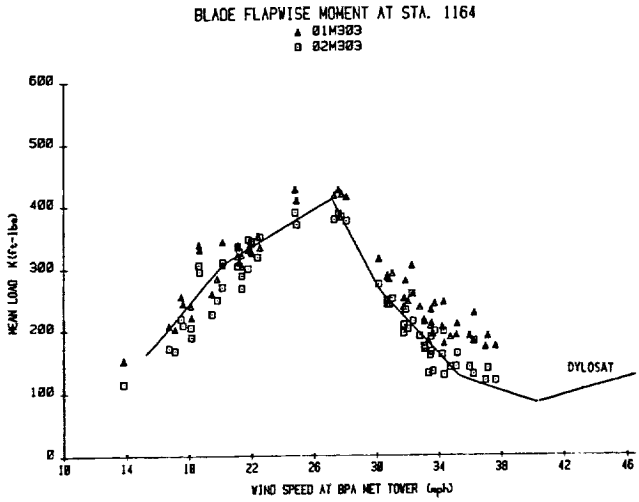

Figure 11. Mean Flapwise Moment at Sta. 1164 (Unit #3, 70% VG)

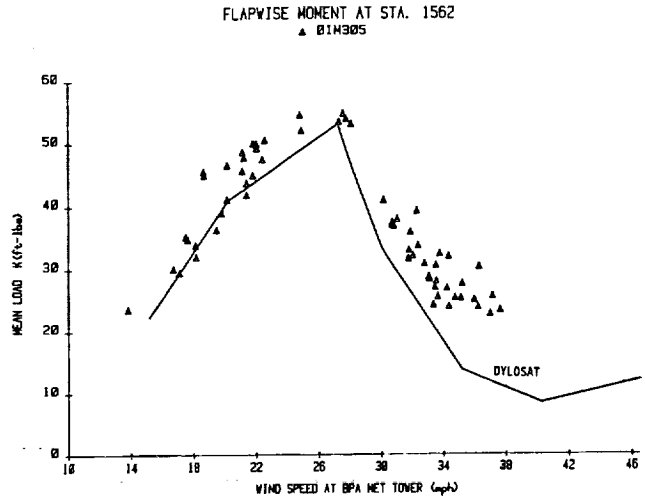

Figure 12. Mean Flapwise Moment at Sta. 1562 (Unit #3, 70% VG)

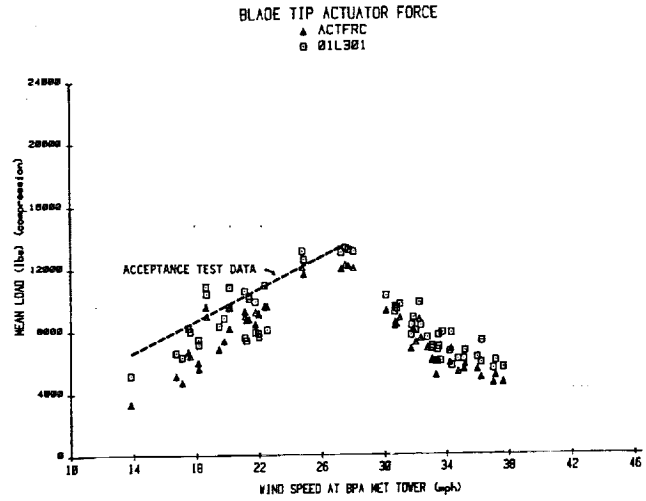

Figure 13. Mean Blade Tip Actuator Force (Unit #3, 70% VG)

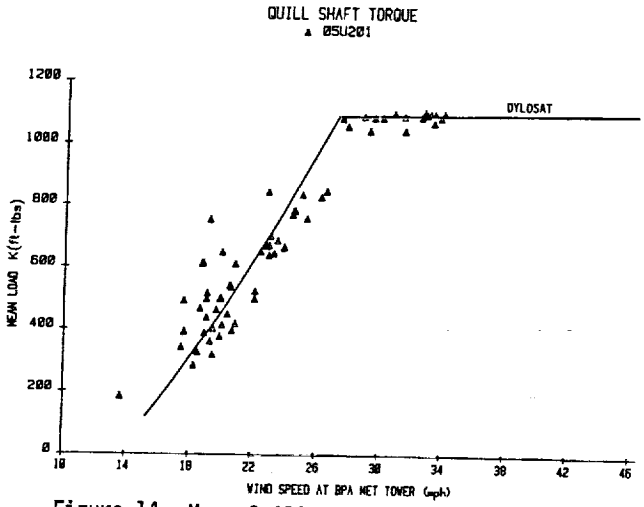

Figure 14. Mean Quill Shaft Torque (Unit #2, 70% VG)

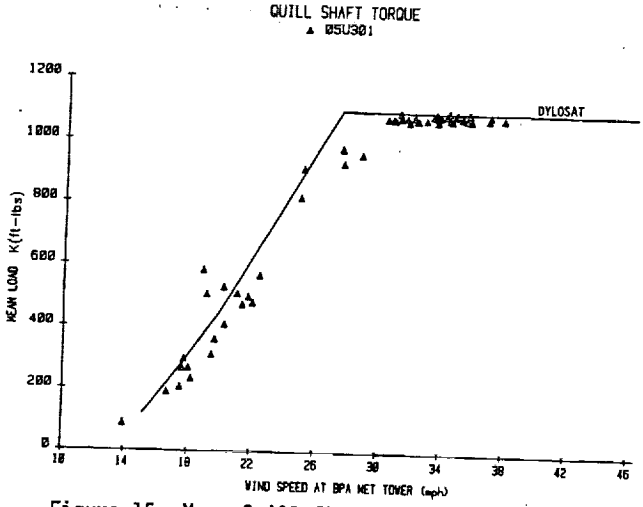

Figure 15. Mean Quill Shaft Torque (Unit #3, 70% VG)

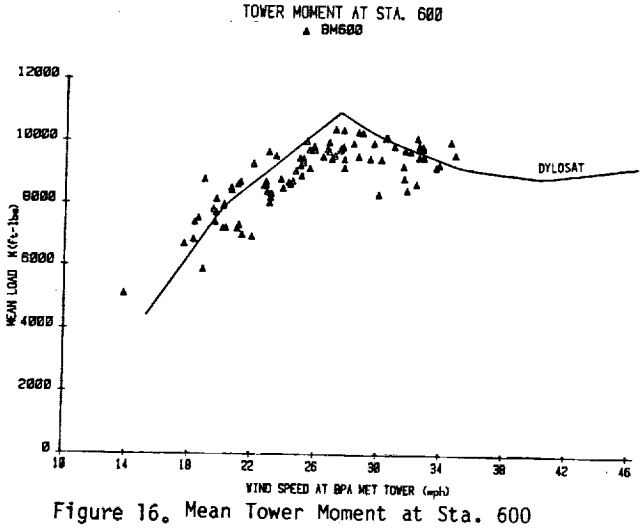

Figure 16. Mean Tower Moment at Sta. 600 (Unit #2, 70% VG)

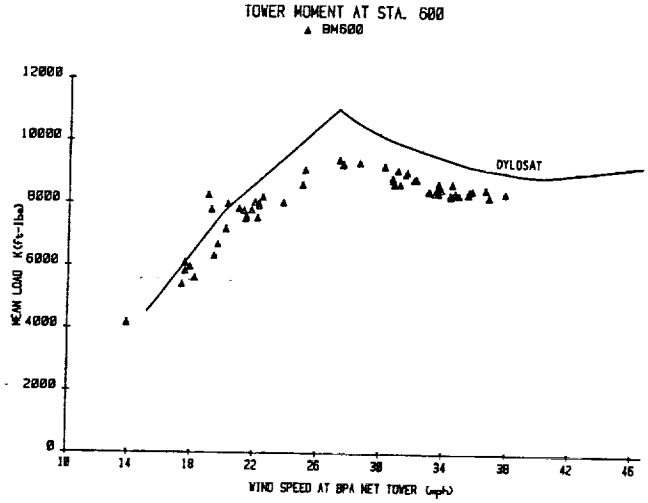

Figure 17. Mean Tower Moment at Sta. 600 (Unit #3, 70% VG)

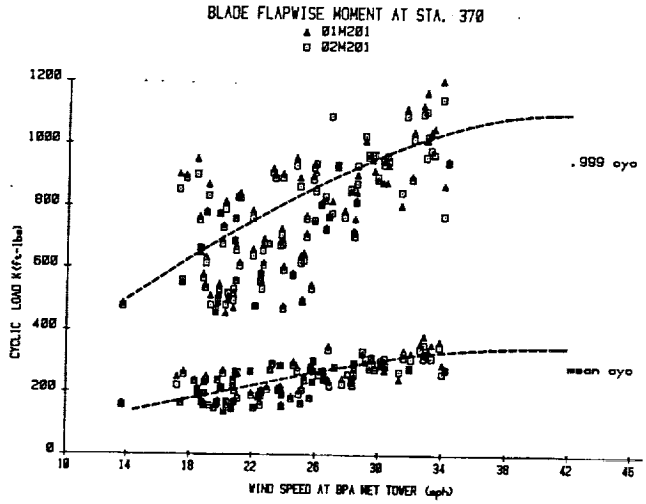

Figure 18. Cyclic Flapwise Moments at Sta. 370 (Unit #2, 70% VG)

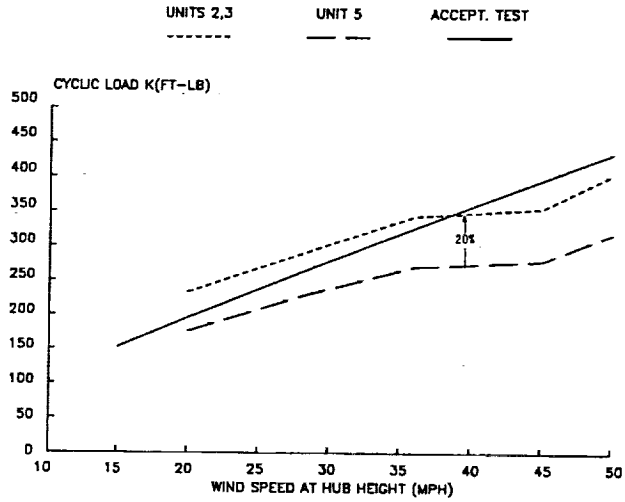

Figure 19. Comparison of Mean Cyclic Flapwise Moment at Sta. 370

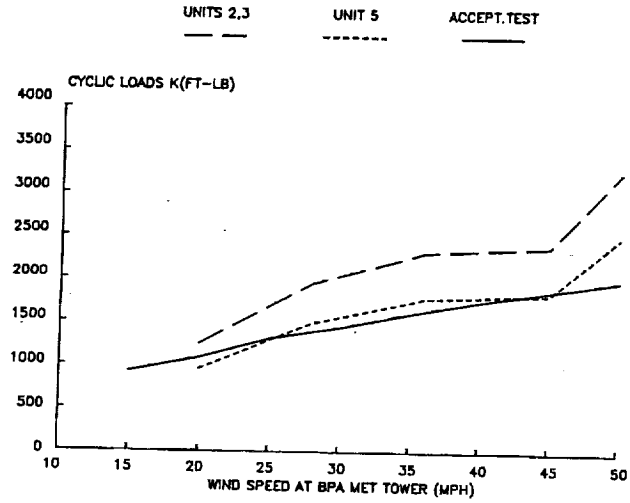

Figure 20. Comparison of Mean Cyclic Tower Moment at Sta. 600

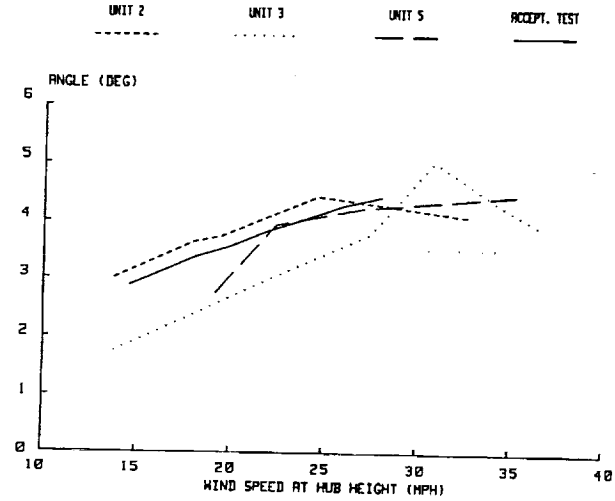

Figure 21. Comparison of Cyclic Teeter Angle

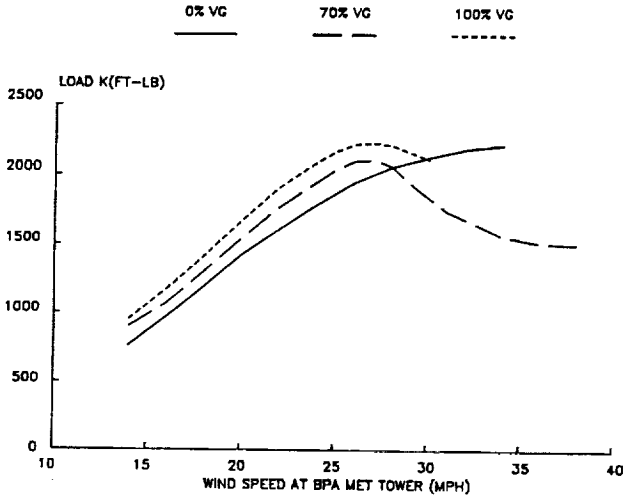

Figure 22. Effect of VG on Mean Flapwise Moment at Sta. 370 (Unit #3)

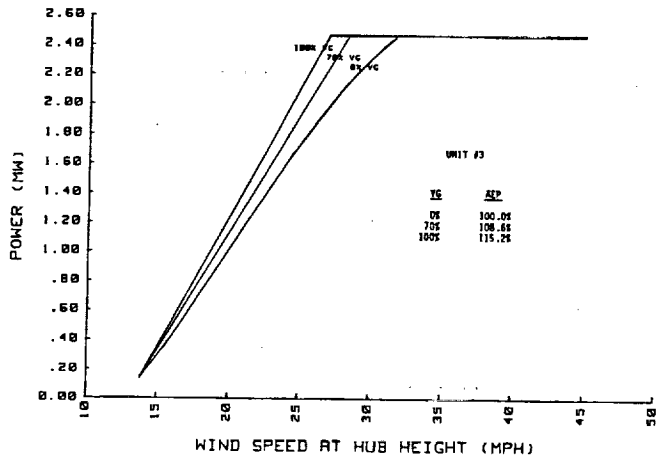

Figure 23. Effect of VG on Performance (Unit #3)

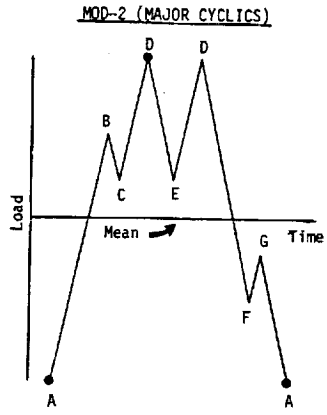

Figure 24. Mod-2 Fatigue Load Cycle Counting Procedure

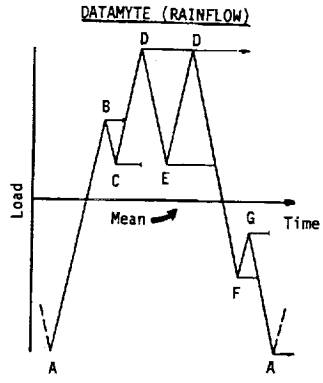

Figure 25. Rainflow Fatigue Load Cycle Counting Procedure

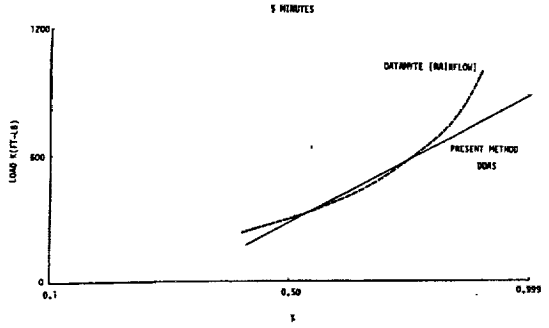

Figure 26. Cumulative Distribution of Cyclic Flapwise Moment at Sta. 370 for Datamyte and Present Method (5 min. sample)

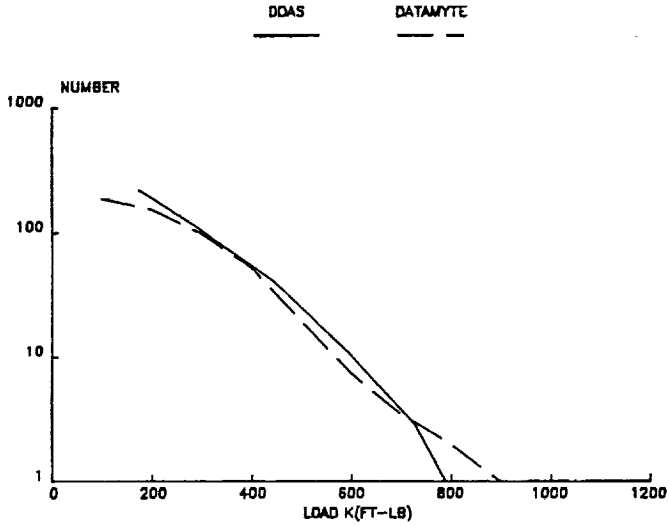

Figure 27. Exceedance Plot of Cyclic Flapwise Moment at Sta. 370

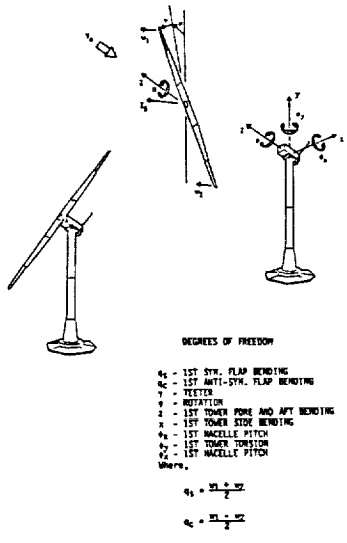

Figure 28. DYLOSAT Model of a Two-Bladed Wind Turbine

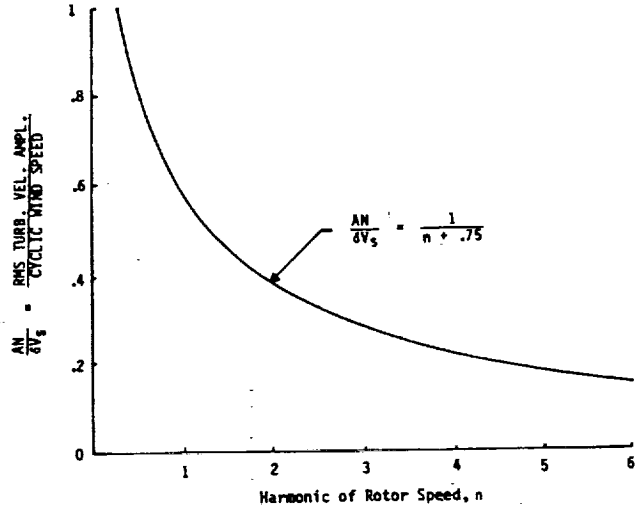

Figure 29. NASA Interim Turbulence Normalized Spectrum

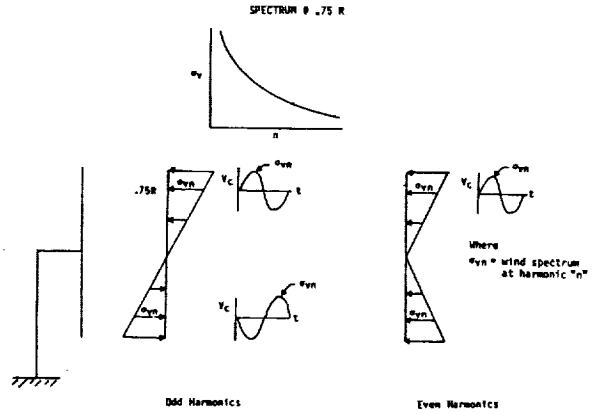

Figure 30. Conceptual Description of the NASA Interim Turbulence Model

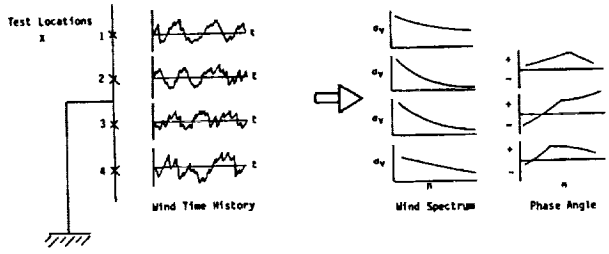

Figure 31. Conceptual Rotationally Sampled Wind Model

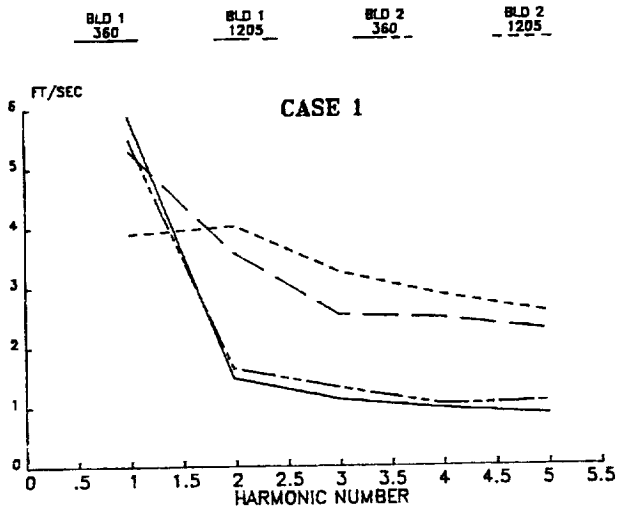

Figure 32. Rotationally Sampled Wind Spectra

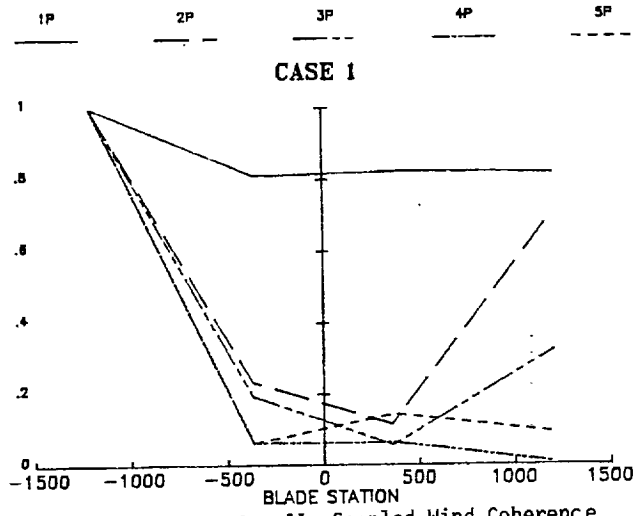

Figure 33. Rotationally Sampled Wind Coherence

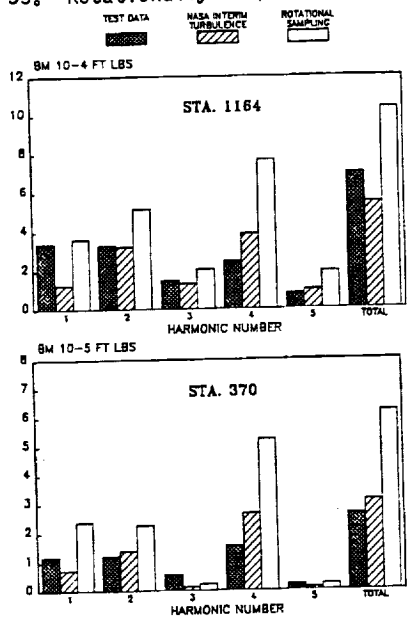

Figure 34. Rotor RMS Bending Moment - Case 1

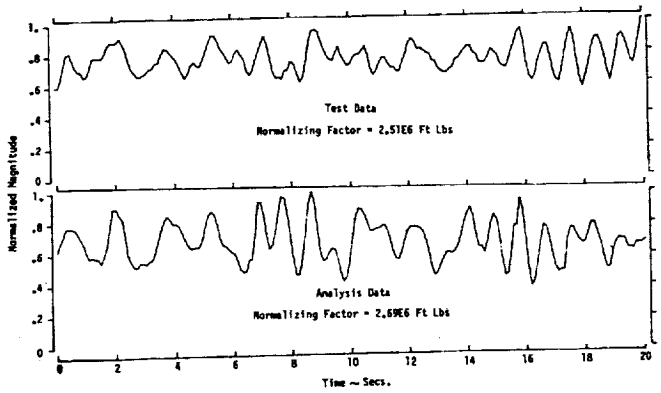

Figure 35. Bending Moment Time History at Rotor Station 370

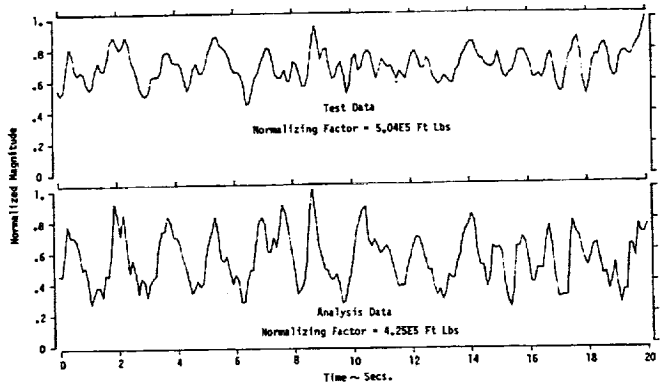

Figure 36. Bending Moment Time History at Rotor Station 1164

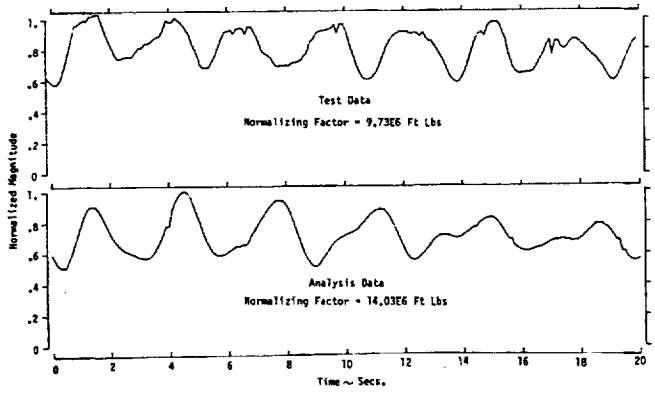

Figure 37. Bending Moment Time History at Tower Station 600

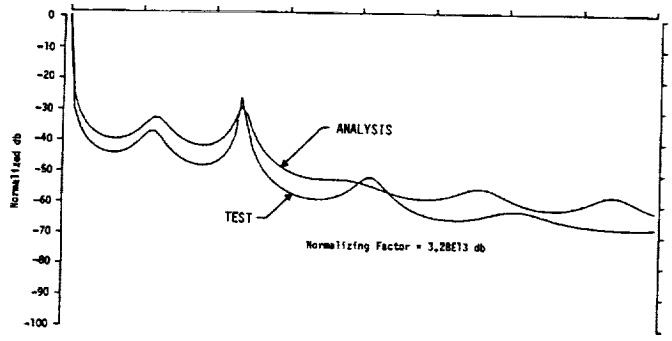

Figure 38. Spectral Analysis of Bending Moment Time History at Rotor Station 370

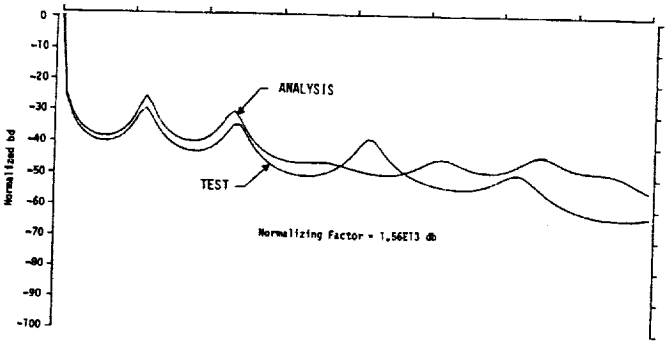

Figure 39. Spectral Analysis of Bending Moment Time Time History at Rotor Station 1164

Table 1

Rotationally Sampled Wind Test Conditions

Case 1			
	Date: 8/4/83	21:22 PST	V_{mean} = 32.2 MPH
Case 2			
	Date: 8/5/83	17:03 PST	V_{mean} = 21.0 MPH
Case 4			
	Date: 8/10/83	12:51 PST	V_{mean} = 27.1 MPH